

GALACTIC DARK MATTER HALOS AND GLOBULAR CLUSTER POPULATIONS. III: EXTENSION TO EXTREME ENVIRONMENTS

WILLIAM E. HARRIS¹, JOHN P. BLAKESLEE², AND GRETCHEN L. H. HARRIS³

(Dated: January 19, 2017)
to be submitted to ApJ

ABSTRACT

The total mass M_{GCS} in the globular cluster (GC) system of a galaxy is empirically a near-constant fraction of the total mass $M_h \equiv M_{\text{bary}} + M_{\text{dark}}$ of the galaxy, across a range of 10^5 in galaxy mass. This trend is radically unlike the strongly nonlinear behavior of total stellar mass M_* versus M_h . We discuss extensions of this trend to two more extreme situations: (a) entire clusters of galaxies, and (b) the Ultra-Diffuse Galaxies (UDGs) recently discovered in Coma and elsewhere. Our calibration of the ratio $\eta_M = M_{\text{GCS}}/M_h$ from normal galaxies, accounting for new revisions in the adopted mass-to-light ratio for GCs, now gives $\eta_M = 2.9 \times 10^{-5}$ as the mean absolute mass fraction. We find that the same ratio appears valid for galaxy clusters and UDGs. Estimates of η_M in the four clusters we examine tend to be slightly higher than for individual galaxies, but more data and better constraints on the mean GC mass in such systems are needed to determine if this difference is significant. We use the constancy of η_M to estimate total masses for several individual cases; for example, the total mass of the Milky Way is calculated to be $M_h = 1.1 \times 10^{12} M_\odot$. Physical explanations for the uniformity of η_M are still descriptive, but point to a picture in which massive, dense star clusters in their formation stages were relatively immune to the feedback that more strongly influenced lower-density regions where most stars form.

Subject headings: galaxies: formation — galaxies: star clusters — globular clusters: general

1. INTRODUCTION

Two decades ago, Blakeslee et al. (1997) used observations of ~ 20 brightest cluster galaxies (BCGs) to propose that the number of globular clusters (GCs) in giant galaxies is directly proportional to the total mass M_h of the host galaxy, which in turn is dominated by the dark matter (DM) halo. This suggestion was followed up with increasing amounts of observational evidence in several papers, including McLaughlin (1999b); Blakeslee (1999); Spitler & Forbes (2009); Georgiev et al. (2010); Kruijssen (2015), Hudson et al. (2014) (hereafter Paper I), Harris et al. (2015) (hereafter Paper II), and Forbes et al. (2016), among others (see Paper II for a more complete review of the literature). This remarkable trend may be a strong signal that the formation of GCs, most of which happened in the redshift range $8 \gtrsim z \gtrsim 2$, was relatively resistant to the feedback processes that hampered field-star formation (e.g. Kravtsov & Gnedin 2005; Moore et al. 2006; Li et al. 2016). If that is the case, then the total mass inside GCs at their time of formation may have been closely proportional to the original gas mass present in the dark-matter halo of their parent galaxy (Papers I, II, and Kruijssen 2015), very unlike the total stellar mass M_* .

Blakeslee et al. (1997) introduced the *number* ratio $\eta_N \equiv N_{\text{GC}}/M_h$ (where N_{GC} is the total number of GCs in a galaxy) and showed that it was approximately constant for their sample of BCGs, at least when measured

within a fixed physical radius. Following Spitler & Forbes (2009), Georgiev et al. (2010), and our Papers I and II in this series, here we discuss the link between GC populations and galaxy total mass in terms of the dimensionless *mass* ratio $\eta_M \equiv M_{\text{GCS}}/M_h$, where M_{GCS} is the total mass of all the GCs combined and M_h is the total galaxy mass including its dark halo plus baryonic components. In some sense, η_M represents an absolute efficiency of GC formation, after accounting for subsequent dynamical evolution up to the present day (cf. Katz & Ricotti 2014; Kruijssen 2015; Forbes et al. 2016). Direct estimates of η_M for several hundred galaxies indicate that this ratio is indeed nearly uniform (Papers I and II), far more so than the more well known ratio M_*/M_h . A second-order dependence on galaxy type has been found in the sense that S/Irr galaxies have a $\sim 30\%$ lower η_M than do E/S0 galaxies (Paper II).

So far, the case that $\eta_M \simeq \text{const}$ has been built on the observed GC populations in ‘normal’ galaxies covering the range from dwarfs to giants. However, opportunities have recently arisen to extend tests of its uniformity in two new directions. The first is by using the GC populations in entire clusters of galaxies, including their GCs in the Intracluster Medium (ICM). The second is from the newly discovered ultra-diffuse galaxies (UDGs) and the GCs within them. It is also worth noting that in both these cases, the masses of the systems concerned have been measured with different methods than by the gravitational-lensing approach used to build the calibration of η_M in our Papers I and II, which makes the test of the hypothesis even more interesting.

The plan of this paper is as follows. In Section 2, we describe improved methodology for determining M_{GCS} , followed by a recalibration of the mass ratio η_M . In Section 3 the discussion is extended to include four clusters

¹ Department of Physics & Astronomy, McMaster University, Hamilton, ON, Canada; harris@physics.mcmaster.ca

² Herzberg Astronomy & Astrophysics, National Research Council of Canada, Victoria, BC V9E 2E7, Canada; jblakeslee@nrc-cnrc.gc.ca

³ Dept. of Physics and Astronomy, University of Waterloo, Waterloo, ON N2L 3G1, Canada; glharris@astro.uwaterloo.ca

of galaxies in which measurements now exist for both M_{GCS} and M_h , while in Section 4 the relation is extended in quite a different direction to selected UDGs. In Section 5, the key ratio η_M is applied to several interesting sample cases with accompanying predictions for their GCS sizes. We finish with brief comments about the implications of the constancy of η_M for understanding the conditions of formation for GCs.

2. RECALIBRATION OF THE MASS RATIO: METHOD

The total GCS mass within a galaxy or cluster of galaxies is calculated as

$$M_{GCS} = \int \left(\frac{M}{L}\right) L n(L) dL \quad (1)$$

where $n(L)$ represents the number of GCs per unit luminosity L , and M/L is their mass-to-light ratio. Here, we use V -band luminosities L_V following most previous studies. The GC luminosity function (GCLF) is assumed to have a Gaussian distribution in number per unit magnitude. The parameters defining $n(L)$, namely the Gaussian turnover magnitude μ_0 and intrinsic dispersion σ , are in turn weak functions of galaxy luminosity, as described in Villegas et al. (2010); Harris et al. (2013, 2014). From the observations covering a large range of host galaxies, μ_0 and σ both exhibit shallow increases as galaxy luminosity increases.

In the present paper, unlike all previous discussions of this topic, we now assume that the mass-to-light ratio M/L_V for individual GCs is also a function of GC mass, following empirical evidence from recent literature (e.g. Rejkuba et al. 2007; Kruijssen 2008; Kruijssen & Mieske 2009; Strader et al. 2011). Of necessity, however, we assume that M/L follows the same function of GC mass (or luminosity, which is the more easily observable quantity) within all galaxies.

In the Appendix below, we assemble recent observational data and define a convenient interpolation function for M/L_V versus GC luminosity. Using Eq. 1, we can then readily derive a mean mass-to-light ratio averaged over all GCs in any given galaxy, defined as $\langle M/L_V \rangle (tot) = M_{GCS}/L_{GC}(tot)$. We can also define a mean GC mass as $\langle M_{GC} \rangle = M_{GCS}/N_{GC}$.⁴ For example, for a typical L_* galaxy at $M_V^T \simeq -21.4$ (the type of galaxy within which most GCs in the universe are found; see Harris 2016), we obtain $\langle M/L_V \rangle \simeq 1.73$. The mean ranges from $\langle M/L_V \rangle \simeq 1.3$ for very small dwarfs ($M_V^T \sim -15$) up to $\langle M/L_V \rangle \simeq 2.1$ for very luminous supergiants ($M_V^T \sim -23$).

In Figure 1 the trends of GC mean mass and global $\langle M/L_V \rangle$ are plotted versus galaxy luminosity M_V^T . Accurate numerical approximations to these results are given by the interpolation curves

$$\log \langle M_{GC} \rangle = 5.698 + 0.1294 M_V^T + 0.0054 (M_V^T)^2 \quad (2)$$

and

$$\log \langle M/L_V \rangle = 1.041 + 0.117 M_V^T + 0.0037 (M_V^T)^2. \quad (3)$$

⁴ By convention, to maintain a consistent calculation procedure, the GCLF is assumed to be Gaussian and N_{GC} is defined for our purposes as twice the number of GCs brighter than the GCLF turnover point; see Harris et al. (2013).

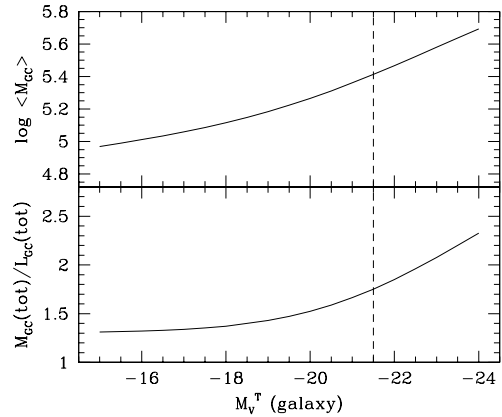


Figure 1. *Upper panel:* Mean GC mass (in Solar units) versus host galaxy luminosity M_V^T . *Lower panel:* Mean mass-to-light ratio for the GCs within a galaxy of luminosity M_V^T , defined as the total mass $M_{GC}(tot)$ in all GCs divided by the total luminosity $L_V(tot)$ of the GCs. The vertical dashed line at $M_V^T = -21.5$ marks L_* galaxies similar to the Milky Way.

The intrinsic galaxy-to-galaxy scatter in $\langle M_{GC} \rangle$ is ± 0.2 dex, based on the observations from the Virgo and Fornax clusters (Villegas et al. 2010).

We have used these calibrations to recalculate the values of M_{GCS} and η_M in the complete sample of galaxies discussed in Papers I and II. In particular, for this paper we use these recalibrated values for the 175 ‘best’ galaxies of all types used in Paper II.⁵ In addition, to help tie down the high-mass end of the range of galaxies, we have updated the N_{GC} values for five Brightest Cluster Galaxies (BCGs) including NGC 4874, 4889, 6166, UGC 9799, and UGC 10143 from the recent data of Harris et al. (2016, ApJ in press).

The results are shown in Figure 2. First, the upper panel shows the *number* per unit mass η_N versus M_h (following the notation convention of Georgiev et al. 2010). An unweighted least-squares fit to the E/S0 galaxies gives the simple linear relation

$$\log \eta_N = (-8.56 \pm 0.34) - (0.11 \pm 0.03) \log(M_h/M_\odot). \quad (4)$$

Thus the total number of GCs in galaxies, observed at redshift 0, scales approximately as $N_{GC} \sim M_h^{0.9}$. The rms scatter around this relation is ± 0.26 dex.

Second, the lower panel shows the trend for the *mass* ratio η_M . Because the *mean mass* of the GCs increases

⁵ This ‘best’ sample consists of all the galaxies for which the raw GC photometry was of high enough quality to separate the conventional red and blue GC subpopulations. In most cases this criterion also means that the limiting magnitude of the photometry was faint enough to be near the GCLF turnover, making the calculation of the total population N_{GC} relatively secure.

progressively with galaxy mass, the shallow decrease of η_N with M_h nearly cancels, leaving the mass ratio η_M approximately constant over the entire run of galaxies. The weighted mean is $\langle \log \eta_M \rangle = -4.54$, or $\langle \eta_M \rangle = 2.9 \times 10^{-5}$, with a residual rms scatter ± 0.28 dex.

In Fig. 2, the lower panel (η_M) and the upper panel (η_N) are obviously closely linked, but they are not entirely equivalent. As described in Paper I, M_h is deduced from the K -band luminosity M_K as calibrated through gravitational lensing. On the other hand, M_{GCS} is derived from N_{GC} and the visual luminosity M_V^T through Eq. (1).

Five points near $M_h \sim 10^{13} M_\odot$ sit anomalously high above the mean relations. These five are NGC 4636 and the BCGs NGC 3258, 3268, 3311, 5193. The cluster populations for these systems are well determined and very unlikely to be overestimated by the factor of ~ 5 that would be needed to bring them back to the mean lines. The alternate possibility is that their halo masses may have been underestimated, which in turn means that the K -band luminosities of these very large galaxies (from 2MASS; see Harris et al. 2013) would have to be underestimated (see Schombert & Smith 2012; Scott et al. 2013, for more extensive comments in this direction).

3. CLUSTERS OF GALAXIES

Useful estimates of the total GC populations within entire clusters of galaxies have now been made for four rich clusters: Virgo, Coma, Abell 1689, and Abell 2744 (sources listed below). This material has in each case taken advantage of wide-field surveys or unusually deep sets of images taken with HST. The quoted N_{GC} values include both the GCs associated directly with the individual member galaxies, and the intracluster globular clusters (IGCs) that are now known to be present in rich clusters. It is likely that the IGCs represent GCs stripped from many different systems during the extensive history of galaxy/galaxy merging and harassment that takes place within such environments (Peng et al. 2011). Simulations (e.g. Purcell et al. 2007) show that L_* -type galaxies contribute the most to the intracluster light. For such galaxies the mean globular cluster mass is $\langle M_{GC} \rangle \simeq 2.6 \times 10^5 M_\odot$ (Fig. 1), and the GCLF mean and dispersion are $\mu_0(M_V) = -7.4$, $\sigma = 1.2$ mag (Harris et al. 2013). However, the total GC population in the entire cluster of galaxies consists of the IGCs plus the individual galaxies in roughly similar amounts. For the giant ellipticals and BCGs that dominate the individual galaxies, the GCLFs are broader with $\sigma \simeq 1.4$ and $\langle M_{GC} \rangle$ is higher. For the present purpose, we therefore adopt averages $\sigma \simeq 1.3$ mag and $\langle M_{GC} \rangle \simeq 2.8 \times 10^5 M_\odot$ for an entire galaxy cluster. Knowing N_{GC} , the total mass M_{GCS} in all the GCs within the cluster can then be directly estimated, albeit with more uncertainty than for a single galaxy.

Virgo: Durrell et al. (2014), from the Next Generation Virgo Cluster Survey, calculate that the entire cluster contains (37700 ± 7500) GCs brighter than $g_0 = 24.0$, which is 0.2 mag fainter than the GCLF turnover point. Adopting the fiducial value $\sigma = 1.3$ mag as explained above, we then obtain $N_{GC} = (67000 \pm 13000)$, which then gives $M_{GCS} = (1.88 \pm 0.37) \times 10^{10} M_\odot$. Durrell et al. also quote a total Virgo mass $5.5 \times 10^{14} M_\odot$, leading to

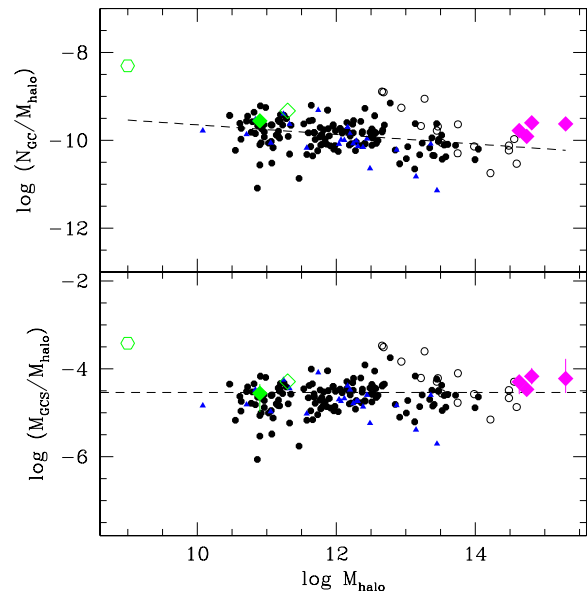


Figure 2. *Upper panel:* Log of the ratio $\eta_N = N_{GC}/M_h$, plotted versus total galaxy mass M_h . *Solid dots:* E/S0 galaxies. *Open circles:* BCGs. *Blue triangles:* S/Irr galaxies. *Magenta diamonds:* The four clusters of galaxies discussed in the text. *Green diamonds:* The ultra-diffuse galaxies. The open diamond for Dragonfly 44 in the Coma cluster is very uncertain (see text). *Green hexagon:* the Fornax dSph satellite of the Milky Way. The dashed line is the least-squares fit defined in the text. *Lower panel:* Log of the mass ratio $\eta_M = M_{GCS}/M_h$ versus M_h ; symbols are the same as in the upper panel. The dashed line is the mean value $\langle \log \eta_M \rangle = -4.54$.

$\eta_M = (3.4 \pm 0.7) \times 10^{-5}$. This η_M estimate is 17% higher than the value quoted by Durrell et al. (2014), but the increase results entirely from the difference in assumed $\langle M_{GC} \rangle$. Just as for the Coma survey data (discussed below), in this case the limiting magnitude of the survey is close to the GCLF turnover (peak) magnitude, so that approximately half the total GC population is directly observed, and the estimated N_{GC} count is virtually independent of the assumed GCLF dispersion σ .

Coma: Peng et al. (2011) find that within a projected radius of $r \simeq 520$ kpc, the cluster contains 71000 ± 5000 GCs (here we combine their estimates of internal and systematic uncertainties, and renormalize the total to $\sigma = 1.3$ mag instead of their value of 1.37 mag), and thus $M_{GCS} = (1.99 \pm 0.14) \times 10^{10} M_\odot$. This survey radius is well within the Coma virial radius, which is 2.5 – 3.0 Mpc (e.g. Hughes 1989; Colless & Dunn 1996; Rines et al. 2003; Lokas & Mamon 2003; Kubo et al. 2007; Gavazzi et al. 2009; Okabe et al. 2014; Falco et al. 2014). From these sources, which use methods including X-ray light, galaxy dynamics, weak lensing, and galaxy sheets to derive the Coma mass profile, the mass within

the GC survey radius of 520 kpc is $M \simeq (4 \pm 1) \times 10^{14} M_{\odot}$. The resulting mass ratio *within this radius* is then $\eta_M = (4.98 \pm 1.25) \times 10^{-5}$.

A1689: Alamo-Martínez et al. (2013) used unusually deep HST imaging of the core region of this massive cluster, which is at redshift $z = 0.183$, to find a large and extended population of GCs. In contrast to Virgo and Coma, the limiting magnitude of their photometry was 2.3 mag brighter than the expected GCLF turnover and thus only the brightest 4.0% of the GC population was measurable. From an analysis of the known statistical and systematic uncertainties, they deduced $N_{GC} = 162,850 (+75,450, -51,300)$ GCs within a projected 400-kpc radius of the central cD-type galaxy after using a GCLF-extrapolated fit to the observed number of GCs brighter than the photometric limit. However, that number assumed $\sigma = 1.4$ mag; converting to our fiducial $\sigma = 1.3$ mag, the total becomes $N_{GC} = 209,600 (+97,100, -66,000)$ within $r < 400$ kpc. From gravitational lensing, the total mass within the same radius is $M_h = 6.4 \times 10^{14} M_{\odot}$. The resulting mass ratio is then $\eta_M(r < 400\text{kpc}) = 9.17(+4.25, -2.90) \times 10^{-5}$. We can attempt to define something closer to a global value out to larger radius by extrapolating the best-fit $r^{1/4}$ -law derived to the full GC distribution in A1689 (their fit for the case without masking the regions around the galaxies), which suggests that the estimated number of GCs out to 1 Mpc is larger by a factor of 1.48. From the multi-probe mass profile of Umetsu et al. (2015, using $h = 0.7$), the total mass within the same radius is $M_h = 1.3 \times 10^{15} M_{\odot}$. We therefore estimate, for the whole cluster, $\eta_M = 6.7(+3.1, -2.1) \times 10^{-5}$ within $r < 1$ Mpc. The total mass of A1689 out to the virial radius exceeds $2 \times 10^{15} M_{\odot}$, and thus the global value of η_M might be still lower. In any case, given the uncertainties, the value of η_M in A1689 appears consistent with the standard range calculated above.

A2744: Lee & Jang (2016) have used HST imaging from the HST Frontier Field to find the brightest GCs and UCDS in this very rich cluster, which is at redshift $z = 0.308$. Intracluster Light (ICL) is also detectably present at least in the inner part of the cluster (Montes & Trujillo 2014). From M. G. Lee (private communication), the raw number of observed GCs brighter than *F814W* = 29.0, after photometric completeness correction, field subtraction and removal of UCDS, is (664 ± 41) (Poisson uncertainty). This limiting magnitude is $\simeq 3.8$ mag brighter than the GCLF turnover point, or 2.93σ short of the turnover. Here, we have adopted a 0.2-mag brightening of the GCLF turnover luminosity to account for passive evolution for its redshift of $z = 0.3$; note that Alamo-Martínez et al. (2013) determined a net brightening in *F814W* of 0.12 mag in A1689 ($z = 0.18$), and for small z the correction scales nearly linearly. Extrapolating from the observed total, then $N_{GC} \simeq 390,000$.

Given that only $\sim 0.2\%$ of the inferred total was actually detected, the dominant sources of error in this case are not the internal count statistics, but instead the uncertainties in the adopted GCLF turnover and dispersion, as well as the basic assumption that the GCLF follows a strictly Gaussian shape all the way to luminosities far above the turnover magnitude. These uncertainties are unimportant for situations like Virgo

and Coma where the raw observations reach to limiting magnitudes approaching the turnover magnitude μ_0 , but they become critically important where only the bright tip of the GCLF is observed. The turnover μ_0 exhibits an intrinsic galaxy-to-galaxy scatter at the level of ± 0.2 mag, while the dispersion σ has an intrinsic scatter of $\pm 0.05 - 0.1$ mag (Jordán et al. 2006; Villegas et al. 2010; Rejkuba 2012). For the baseline values of $\sigma(\text{GCLF}) = 1.3$ mag and a limiting magnitude 2.93σ brighter than the turnover, the fraction $N(\text{obs})/N(\text{tot})$ equals 0.0017 ($+0.0010, -0.00066$) due to a ± 0.2 -mag uncertainty in the turnover luminosity, and an additional ($+0.00166, -0.00094$) due to a ± 0.1 -mag uncertainty in σ . Treating the uncertainties as independent, we obtain $N_{GC} = 3.9(+7.2, -2.1) \times 10^5$. If we further assume the GC counts extend out to 600 kpc (the limit that can be probed within the ACS field of view at this redshift) and follow a similar profile to that of A1689, then the correction to a radius of 1 Mpc is a factor of 1.21, **yielding** $N_{GC} = 4.7(+8.6, -2.5) \times 10^5$.

The best-estimate mass of A2744 is also difficult to pin down, since the cluster has complex internal dynamics with two major subclusterings at quite different mean velocities, indicative of merging in progress (Boschin et al. 2006; Owers et al. 2011; Jauzac et al. 2016). For the dominant central "a" subcluster Boschin et al. (2006) determine $M_{vir}(< 2.4\text{Mpc}) = 2.2(+0.7, -0.6) \times 10^{15} M_{\odot}$. With this value for the mass, we conclude $\eta_M = 6.0(+11, -3.2) \times 10^{-5}$ for A2744.

The underlying assumption about the Gaussian GCLF shape is harder to quantify. The strongest empirical test available is the measurement of GCLFs in seven BCG galaxies from Harris et al. (2014), which extend from the turnover point to an upper limit almost 5 magnitudes brighter (equivalent to almost 4σ), thanks to the extremely large numbers of GCs per galaxy. The results indicate that the Gaussian assumption fits the data remarkably well to that level. However, these tests all apply to *single* galaxies, whereas the IGCs are a composite population of GCs stripped from galaxies of all types. This composite GCLF will in general not have a simple Gaussian shape even if all the progenitor galaxies had individually normal GCLFs (see Gebhardt & Beers 1991). Unfortunately, no direct measurements of the GCLF for a pure IGC population are yet available. For the present time, we simply adopt the parameters for galaxy clusters as described above and recognize that further observations and analysis could change the results for A2744 quite significantly. While uncertainties are also sizable for A1689, the fraction of the GC population directly observed there is 20 to 40 times greater than in A2744; thus, the results for A1689 are robust by comparison.

It is evident from the preceding discussion that estimates of η_M on the scale of entire clusters of galaxies put us in a much more challenging regime of uncertainties than is the case for single galaxies. In particular, better results will be possible if η_M as a function of r can be more accurately established. Ideally the global value should be estimated out to the virial radius, but so far this is the case only for Virgo, the cluster for which the estimated η_M is closest to the mean for individual galaxies. Nevertheless, for all four galaxy clusters, the weighted average result is $\eta_M = (3.9 \pm 0.6) \times 10^{-5}$, slightly

larger than the mean value of 2.9×10^{-5} characterizing the individual galaxies. It is difficult to say at this point whether or not the mean difference is significant. One possible evolutionary difference between the GCs within galaxies and the IGCs is that the IGCs are subjected to much lower rates of dynamical destruction than the GCs deep within the potential wells of individual galaxies, and so may have kept a higher fraction of their initial mass.

4. ULTRA-DIFFUSE GALAXIES

UDGs have recently been found within the Virgo, Fornax, and Coma clusters in large numbers (e.g. Mihos et al. 2015; van Dokkum et al. 2015; Koda et al. 2015; Muñoz et al. 2015). Deep imaging has revealed GC populations around two of the Coma UDGs, Dragonfly 44 (van Dokkum et al. 2016) and Dragonfly 17 (Peng & Lim 2016), as well as VCC1287 in Virgo (Beasley et al. 2016). All three of these systems have anomalously high specific frequencies $S_N \sim N_{GC}/L_V$, but the interest for this discussion is their *mass* ratio. Beasley et al. (2016) and van Dokkum et al. (2016) have already commented that η_M for the two UDGs they studied falls close to the standard level applicable for more normal galaxies.

For the Virgo dwarf VCC1287, Beasley et al. (2016) find a GC population $N_{GC} = 22 \pm 8$, which would translate to $M_{GCS} = (2.2 \pm 0.8) \times 10^6 M_\odot$ if we adopt a mean GC mass of $1.0 \times 10^5 M_\odot$ appropriate for a moderate dwarf galaxy. Fortunately, $\langle M_{GC} \rangle$ does not vary strongly across the dwarf luminosity range (see Fig. 1). From a combination of the velocity dispersion of the GCs themselves, and comparison with EAGLE simulations, they estimate a virial mass for the galaxy of $M_{200} = (8 \pm 4) \times 10^{10} M_\odot$, giving an approximate mass ratio $\eta_M = (2.75 \pm 1.70) \times 10^{-5}$.

For Dragonfly 44, van Dokkum et al. (2016) find a relatively rich GC population $N_{GC} \simeq 94 \pm 25$ and, again, a specific frequency S_N higher by an order of magnitude than normal galaxies with similar L_V . With $\langle M_{GC} \rangle = 1.1 \times 10^5 M_\odot$ for the galaxy luminosity $M_V^T = -16.1$, then $M_{GCS} = (1.0 \pm 0.3) \times 10^7 M_\odot$. Their measurement of the velocity dispersion of the stellar light gives $M(< r_{1/2}) = 7.1 \times 10^9 M_\odot$. The total (virial) mass M_h is likely to be at least an order of magnitude higher, but scaling from the comparable results for VCC1287 above (see Beasley et al. 2016), we obtain a *very* rough estimate $M_h \sim 2 \times 10^{11} M_\odot$. In turn, the final result is $\eta_M \sim 5.5 \times 10^{-5}$, again very uncertain.

5. DISCUSSION AND CONCLUSIONS

From Fig. 2, we find that the near-constancy of the mass ratio η_M over 5 orders of magnitude in M_h remains valid. The addition of two quite different environments to the mix, UDGs and entire galaxy clusters, has not changed the essential result. It is worth noting that the M_h estimates for the galaxy clusters and UDGs relied on internal dynamics rather than the weak-lensing calibration used for the normal galaxies (except A1689, for which the mass is based on a combination of weak and strong lensing). The new calibration of the mean mass ratio $\eta_M = (2.9 \pm 0.2) \times 10^{-5}$ is significantly lower than in previous papers (see Paper II for comparisons); the difference is due mainly to our lower adopted GC mass-to-light ratio and its nonlinear dependence on GC mass.

An additional residual outcome is that the slight nonlinearity in the trend of η_M (see Papers I and II) is now reduced.

5.1. Galaxy Mass Estimation

In a direct practical sense, η_M is usable as a handy way to estimate the total mass of a galaxy (dark plus baryonic) to better than a factor of 2. This direction is the emphasis taken notably by Spitler & Forbes (2009); van Dokkum et al. (2016); Peng & Lim (2016) and Beasley et al. (2016) and was also used in Paper I to apply to M31 and the Milky Way. As these authors emphasize, it remains surprising that a method apparently unconnected with internal satellite dynamics, lensing, or other fairly direct measures of a galaxy's gravitational field can yield such an accurate result. The prescription for determining M_h is:

1. Count the total GC population, N_{GC} . Given the uncertainties discussed in Section 3 above and in Harris et al. (2013), it is important to have raw photometric data that reach or approach the GCLF turnover point, which helps avoid uncomfortably large extrapolations from observations that resolve only the bright tip of the GCLF.
2. Use the galaxy luminosity M_V^T to define the appropriate mean GC mass $\langle M_{GC} \rangle$ (from Fig. 1 and Eq. 2). The total mass in the galaxy's GC system follows as $M_{GCS} = N_{GC} \langle M_{GC} \rangle$.
3. Divide M_{GCS} by η_M to obtain M_h .

More generally, this method for estimating galaxy mass is workable only for systems near enough that the GC population can be resolved and counted. The practical 'reach' of the procedure is $d \lesssim 200 - 300$ Mpc through deep HST imaging (e.g. Harris et al. 2014), though with the use of SBF techniques, the effective limit may be extended somewhat further; cf. Blakeslee et al. (1997); Blakeslee (1999); Marin-Franch & Aparicio (2002).

5.2. Sample Cases

We provide some sample specific examples of the procedure:

Milky Way: Harris (1996) (2010 edition) lists 157 GCs in the Milky Way, but many of these are extremely faint or sparse objects that would be undetectable in almost all other galaxies. To treat this system in the same way as other galaxies, we note that the GCLF turnover is at $M_V \simeq -7.3$ and that there are 72 clusters brighter than that point. Doubling this, we then adopt $N_{GC} = 144$ in the sense that it is defined here. At $M_V^T(MW) \simeq -21.0$ (Licquia et al. 2015; Bland-Hawthorn & Gerhard 2016), close to an L_* galaxy, the mean GC mass is then $\langle M_{GC} \rangle = 2.3 \times 10^5 M_\odot$, from which $M_{GCS} = 3.3 \times 10^7 M_\odot$. Finally then, $M_h \simeq 1.1 \times 10^{12} M_\odot$, which is well within the mix of estimates obtained from a wide variety of methods involving satellite dynamics and Local Group timing arguments (see, e.g. Wang et al. 2015; Eadie & Harris 2016, for compilations and comparisons).

Dragonfly 17: For this UDG in Coma, Peng & Lim (2016) estimate a total population $N_{GC} = 28 \pm 14$ based

on a well sampled GCLF and radial distribution. For $M_V^T = -15.1$, we have $\langle M_{GC} \rangle = 0.94 \times 10^5 M_\odot$ and then predict a total mass $M_h = (9.1 \pm 4.5) \times 10^{10} M_\odot$ for this galaxy. Peng & Lim (2016) predicted $M_h = (9.3 \pm 4.7) \times 10^{10} M_\odot$, although the agreement with our estimate is something of a coincidence: they used a higher value of η from an older calibration, but also a higher mean GC mass, and these two differences cancelled out.

M87: This centrally dominant Virgo giant is the classic “high specific frequency” elliptical. From the GCS catalog (Harris et al. 2013), $N_{GC} = 13000 \pm 800$ and the luminosity is $M_V^T = -22.61$, giving a mean cluster mass $\langle M_{GC} \rangle = 3.4 \times 10^5 M_\odot$. Thus $M_{GCS} = (4.4 \pm 0.3) \times 10^9 M_\odot$, leading to the prediction $M_h = 1.5 \times 10^{14} M_\odot$. For comparison, Oldham & Auger (2016) give $M_{vir} = 7.4(+12.1, -4.1) \times 10^{13} M_\odot$ from the kinematics of the GC system and satellites. A plausible upper limit from McLaughlin (1999a) is $M_{DM}(r_{200}) = (4.2 \pm 0.5) \times 10^{14} M_\odot$, obtained from the GC dynamics and the X-ray gas in the Virgo potential well, while Durrell et al. (2014) quote $5.5 \times 10^{14} M_\odot$ for the entire Virgo cluster. For BCGs it is difficult to isolate the galaxy’s dark-matter halo from that of the entire galaxy cluster, but given that M87 holds $\simeq 20\%$ of the Virgo GC population, these estimates of M_h seem mutually consistent.

Fornax Cluster: Fornax is the next nearest rich cluster of galaxies after Virgo, with the cD giant NGC 1399 near its center. GC populations in the individual galaxies have been studied as part of the HST/ACS Fornax Cluster Survey (Villegas et al. 2010; Jordán et al. 2015), and the NGC 1399 system particularly has been well studied photometrically and spectroscopically (e.g. Dirsch et al. 2003; Schubert et al. 2010). The Fornax cluster as a whole is not as rich as Virgo or the others discussed here, but an ICM is present at least in the form of substructured X-ray gas (Paolillo et al. 2002). Global mass measurements from galaxy dynamics in and around Fornax (Drinkwater et al. 2001; Nasonova et al. 2011) find $M(<1.4 \text{ Mpc}) = (7 \pm 2) \times 10^{13} M_\odot$, rising to perhaps as high as $3 \times 10^{14} M_\odot$ within 3 Mpc. For NGC 1399 itself, Schubert et al. (2010) find M_{vir} approaching $10^{13} M_\odot$. If we use the mean value $\eta_M = 3.9 \times 10^{-5}$ determined above for the other galaxy clusters, and we also use $M_h = 7 \times 10^{13} M_\odot$ within a radius of 1.4 Mpc, then we predict that the entire Fornax cluster should contain at least $N_{GC} \sim 10,000$ clusters. NGC 1399 alone has $N_{GC} = (6450 \pm 700)$ (Dirsch et al. 2003) and the other smaller galaxies together are likely to contribute at least 6000 more (Jordán et al. 2015). Thus the prediction and the actual known total agree to within the internal scatter of η_M , which would indicate that the GC population within Fornax is already accounted for and that few IGCs remain to be found. It will be intriguing to see if wide-field surveys (see, e.g. D’Abrusco et al. 2016) will reveal a significant IGC population.

Fornax dSph: The dwarf spheroidal satellite of the Milky Way, Fornax, is an especially interesting case. It has 5 GCs of its own and a total luminosity of just $M_V^T = -13.4$, placing it among the very faintest galaxies known to contain GCs. Since it lacks a measured K -band luminosity it does not appear in the GCS catalog with a lensing-calibrated M_h . The existence of

this handful of GCs presents something of an interpretive puzzle for understanding their survival over a Hubble time, with several discussions of dynamical modelling in the recent literature (e.g. Cole et al. 2012; Strigari et al. 2006; Peñarrubia et al. 2008; Martinez 2015). The 5 Fornax clusters add up to a total mass $M_{GCS} = 3.8 \times 10^5 M_\odot$ assuming $(M/L_V) = 1.3$ (Mackey & Gilmore 2003). The predicted halo mass of the galaxy should then be $M_h \simeq 1.3 \times 10^{10} M_\odot$ if we adopt our normal η_M , which would give Fornax a global mass-to-light ratio $M_h/L_V(tot) \gtrsim 600$ (assuming that it has kept its entire halo to the present day against tidal stripping from the Milky Way). By contrast, dynamical modelling of Fornax with various assumed dark-matter profiles tends to infer virial masses near $M_h \sim 10^9 M_\odot$ (Peñarrubia et al. 2008; Cole et al. 2012; Angus & Diaferio 2009). In that case, the derived mass ratio would then be $\eta_M \simeq 3.8 \times 10^{-4}$, an order of magnitude larger than our standard value. Fornax is plotted in Fig. 2 with this higher value; although it is not located outrageously far from the scatter of points defined by the larger galaxies, it does leave a continuing problem for interpretation. With $M_h = 10^9 M_\odot$ and our baseline value $\eta_M \sim 3 \times 10^{-5}$, the normal prediction would be that Fornax should contain only one GC.

The Fornax dSph case hints that the argument for a constant η across the range of galaxies may begin to break down at the very lowest luminosities. For a standard $\eta_M \simeq 3 \times 10^{-5}$, the boundary below which dwarf galaxies should be too small to have any remaining GCs is near $M_h \lesssim 3 \times 10^9 M_\odot$. In this very low-mass regime, other physical factors should also come into play determining the number of surviving GCs within the galaxy, particularly massive gas loss during the earliest star-forming period in such tiny potential wells.

5.3. Cluster Formation Conditions

In the longer term, we suggest that the more important implications for the near-constancy of η_M are for helping understand the formation conditions of the dense, massive star clusters that evolved into the present-day GCs (see Papers I and II). These clusters should have formed within very massive host Giant Molecular Clouds (GMCs) under conditions of unusually high pressure and turbulence, analogous to the Young Massive Clusters (YMCs) seen today in starburst dwarfs, galactic nuclei, and merging systems (Harris & Pudritz 1994; Elmegreen et al. 2012; Kruijssen 2015).

Under such conditions, star formation within these dense protoclusters will be shielded from *external* feedback such as active galactic nuclei, UV and stellar winds from more dilute field star formation, and cosmic reionization (e.g. Kravtsov & Gnedin 2005; Li & Gnedin 2014; Howard et al. 2016). In strong contrast, these forms of feedback were much more damaging to the majority of star formation happening in lower-density, lower-pressure local environments. Though such a picture needs more quantitative modelling, it is consistent with the idea (Paper II) that M_{GCS} at high redshift may be nearly proportional to the total initial gas mass – at least, much more so than the total stellar mass M_* .

An alternate route (Kruijssen 2015) is that the empirical result $\eta_M \sim const$ can be viewed in some sense as a

coincidence if it is written as

$$\eta_M = \frac{M_{\text{GCS}}}{M_h} = \frac{M_{\text{GCS}}}{M_\star} \cdot \frac{M_\star}{M_h}. \quad (5)$$

The two ratios on the right-hand side show well known opposite trends with M_h that happen to cancel out when multiplied together. The stellar-to-halo mass ratio (SHMR) (M_\star/M_h) reaches a peak efficiency near $M_h \simeq 10^{12} M_\odot$ and falls off to both higher and lower mass by more than an order of magnitude (Leauthaud et al. 2012; Moster et al. 2013; Behroozi et al. 2010, 2013; Hudson et al. 2015). By contrast, the GCS number per unit M_\star (that is, the specific frequency S_N or its mass-weighted version T_N) reaches a minimum near $M_h \sim 10^{12} M_\odot$ and rises by an order of magnitude on both sides. Both these trends are extremely nonlinear, and we suggest that it is difficult to see how their mutual cancellation can be so exact over such a wide range of galaxy mass if it is only a coincidence.

The common factor between the two mass ratios (T_N , SHMR) is the galaxy stellar mass M_\star . As in Paper II, we suggest that the result can be seen as the outcome of a *single* physical process (the role of galaxy-scale feedback on M_\star). If instead we essentially ignore M_\star , then M_{GCS} is closer to representing the total initial gas mass, and thus M_h . We recognize, however, that this argument is as yet unsatisfactorily descriptive and will require full-scale numerical simulations that track GC formation within hierarchical galaxy assembly over the full range of redshifts $8 \gtrsim z \gtrsim 1$ (Kravtsov & Gnedin 2005; Li et al. 2016; Griffen et al. 2010; Tonini 2013).

5.4. Conclusions

In this paper we have revisited the empirical relation between the total mass M_{GCS} of the globular clusters in a galaxy, and that galaxy’s total mass M_h . Our findings are the following:

1. A recalibration of the mass ratio $\eta_M \equiv$

(M_{GCS}/M_h), now including the systematic trend of GC mass-to-light ratio with GC mass, yields $\langle \eta_M \rangle = 2.9 \times 10^{-5}$ with a ± 0.28 -dex scatter between individual galaxies.

2. Evaluation of η_M for four *clusters of galaxies* (Virgo, Coma, A1689, A2744) including all GCs in both the cluster galaxies and the IGM, shows that very much the same mass ratio applies for entire clusters as for individual galaxies. For these four clusters $\langle \eta_M \rangle = (3.9 \pm 0.6) \times 10^{-5}$.
3. Two of the recently discovered Ultra-Diffuse Galaxies in Virgo and Coma can also now be included in the relation. Within the (large) measurement uncertainties, both such galaxies fall within the normal value of η_M at the low-mass end of the galaxy range. By contrast, the Fornax dSph in the Local Group may be a genuine extreme outlier, containing perhaps 5 times more clusters than expected.
4. The near-constant mass ratio between GC systems and their host galaxy masses is strikingly different from the highly nonlinear behavior of total stellar mass M_\star versus M_h . We favor the interpretation that GC formation – in essence, star formation under conditions of extremely dense gas in proto-GCs embedded in turn within giant molecular clouds – was nearly immune to the violent external feedback that hampered most field star formation.

ACKNOWLEDGEMENTS

WEH acknowledges financial support from NSERC (Natural Sciences and Engineering Research Council of Canada). We are grateful to Myung Gyoon Lee for helpfully transmitting their observed numbers of globular clusters in Abell 2744. JPB thanks K. Alamo-Martínez for helpful discussions about Abell 1689.

APPENDIX

MASS-TO-LIGHT RATIOS FOR GLOBULAR CLUSTERS

A key ingredient in the calculation of M_{GCS} , the total mass in the globular cluster system of a given galaxy, is the assumed mass-to-light ratio M/L_V for GCs. Along with many other GC studies in recent years, we simply used a constant $M/L_V = 2$ in Papers I and II. However, much recent data and modelling for internal dynamical studies of GCs supports (a) a lower mean value, (b) a significant cluster-to-cluster scatter probably because of differing dynamical histories, and (c) a systematic trend for M/L_V to increase with GC mass (or luminosity) particularly for masses above $10^6 M_\odot$.

Figure 3 shows estimates of M/L_V for Milky Way GCs, determined from measurements of GC internal velocity dispersion combined with dynamical modelling. Data from two widely used previous compilations (Mandushev et al. 1991; McLaughlin & van der Marel 2005) are shown in the upper two panels of the Figure. Since then, dynamical studies have been carried out on numerous individual GCs based on both radial-velocity and proper-motion data, that are built on larger and more precise samples than in the earlier eras. Results from these post-2005 studies are listed in Table 1 and plotted in the bottom panel of Fig. 3. (Note that many clusters appear more than once because each individual study is plotted. However, the values listed in Table 1 present the weighted mean M/L_V , in Solar units, for each cluster.) The cluster luminosities M_V^T are from the catalog of Harris (1996) (2010 edition). For the clusters listed in Table 1, the weighted mean value for 36 GCs excluding NGC 5139 and NGC 6535 is $\langle M/L_V \rangle = (1.3 \pm 0.08) M_\odot/L_{V_\odot}$ with a cluster-to-cluster rms scatter of ± 0.45 . For comparison, the values in the upper panel of Fig. 3 have a mean $\langle M/L_V \rangle = (1.49 \pm 0.11) M_\odot/L_{V_\odot}$ with an rms scatter of ± 0.58 , while in the middle panel the mean is $\langle M/L_V \rangle = (1.53 \pm 0.11) M_\odot/L_{V_\odot}$ with an rms scatter of ± 0.64 .

There is also now much new observational material for GC mass measurements in other nearby galaxies. For other galaxies, the spatial structures of the GCs are unresolved or only partially resolved, and the measurements most often consist of a luminosity-weighted average of the internal velocity dispersion of each cluster, converted to mass via some

Table 1
MASS-TO-LIGHT RATIOS FOR MILKY WAY CLUSTERS

Cluster	M/L_V	\pm	M_V^T	Sources
NGC104	1.32	(0.03,0.03)	-9.42	6,15
NGC288	1.53	(0.17,0.17)	-6.75	6,10,15
NGC362	1.10	(0.10,0.10)	-8.43	6,15
NGC2419	1.55	(0.10,0.10)	-9.42	1,15
NGC2808	2.24	(0.19,0.19)	-9.39	6,9
NGC3201	1.91	(0.17,0.17)	-7.45	15
NGC4147	1.47	(0.54,0.54)	-6.17	6
NGC4590	1.40	(0.43,0.43)	-7.38	6
NGC5024	1.38	(0.16,0.16)	-8.72	6,10
NGC5053	1.30	(0.26,0.26)	-6.76	6
NGC5139	2.45	(0.04,0.04)	-10.26	12,13,15
NGC5272	1.32	(0.14,0.14)	-8.88	4,6
NGC5466	0.72	(0.23,0.23)	-6.98	6
NGC5904	1.36	(0.21,0.21)	-8.81	6
NGC6121	1.32	(0.14,0.14)	-7.19	6,15
NGC6205	2.10	(0.27,0.17)	-8.55	4
NGC6218	1.12	(0.10,0.10)	-7.31	6,10,15
NGC6254	1.61	(0.19,0.19)	-7.48	15
NGC6341	1.69	(0.07,0.07)	-8.21	4,6,15
NGC6388	1.45	(0.13,0.13)	-9.41	8,14
NGC6397	1.9	(0.10,0.10)	-6.64	5
NGC6402	1.82	(0.35,0.35)	-9.10	6
NGC6440	1.23	(0.27,0.27)	-8.75	14
NGC6441	1.07	(0.19,0.19)	-9.63	6,14
NGC6528	1.12	(0.39,0.42)	-6.57	14
NGC6535	11.06	(2.68,2.12)	-4.75	14
NGC6553	1.02	(0.31,0.36)	-7.77	14
NGC6656	1.30	(0.13,0.13)	-8.51	6,15
NGC6715	1.52	(0.45,0.45)	-9.98	6
NGC6752	2.65	(0.19,0.19)	-7.73	6,10
NGC6809	0.81	(0.05,0.05)	-7.57	3,6,10,15
NGC6838	1.36	(0.39,0.39)	-5.61	6
NGC6934	1.52	(0.49,0.49)	-7.45	6
NGC7078	1.14	(0.05,0.05)	-9.19	6,11,15
NGC7089	1.66	(0.38,0.38)	-9.03	6
NGC7099	1.84	(0.19,0.19)	-7.45	6,10
Pal 5	1.60	(0.85,0.59)	-5.17	7
Pal 13	2.4	(5.0,2.4)	-3.76	2

Sources: (1) Bellazzini et al. (2012); (2) Bradford et al. (2011); (3) Diakogiannis et al. (2014); (4) Kamann et al. (2014); (5) Kamann et al. (2016); (6) Kimmig et al. (2015); (7) Küpper et al. (2015); (8) Lützgendorf et al. (2011); (9) Lützgendorf et al. (2012); (10) Sollima et al. (2012); (11) van den Bosch et al. (2006); (12) van de Ven et al. (2006); (13) Watkins et al. (2013); (14) Zaritsky et al. (2014); (15) Zocchi et al. (2012).

appropriate form of the virial theorem or mass profile model. Data from several galaxies are displayed in Figure 4, including M31 (Meylan et al. 2001; Strader et al. 2011), M33 (Larsen et al. 2002), NGC 5128 (Martini & Ho 2004; Rejkuba et al. 2007; Taylor et al. 2010), and M87 (Håegagan et al. 2005).

The M/L_V results from these different studies occupy similar ranges as in the Milky Way, but perhaps not surprisingly the scatter is much larger for these fainter targets. Some puzzling issues remain, for example in NGC 5128 for which the Taylor et al. (2010) values are roughly 50% larger than those from Rejkuba et al. (2007) and Martini & Ho (2004) for 14 objects in common, though again with considerable scatter. The source of this discrepancy is unclear. Possible trends of M/L with GC metallicity as deduced from the M31 sample are discussed by Strader et al. (2011); Shanahan & Gieles (2015); Zonoozi et al. (2016) and are also not yet clear.

By contrast, there is general agreement that M/L should increase systematically with GC mass (Kruijssen 2008; Kruijssen & Mieske 2009; Rejkuba et al. 2007; Strader et al. 2011), since the high-mass clusters have relaxation times large enough that the preferential loss of low-mass stars has not yet taken place to the same degree as for lower-mass clusters. The mean M/L_V is expected to increase from $\sim 1 - 2$ at $M < 10^6 M_\odot$ progressively up to the level $\simeq 5 - 6$ for the mass range $10^7 - 10^8 M_\odot$ characterizing UCDS (Ultra-Compact Dwarfs) and dwarf E galaxies (e.g. Baumgardt & Mieske 2008; Mieske et al. 2008). For convenience of later calculation, we define a simple interpolation curve for M/L as a function of cluster luminosity,

$$\frac{M}{L_V} = 1.3 + \frac{4.5}{1 + e^{2.0(M_V^T + 10.7)}}. \quad (\text{A1})$$

This function gives a roughly linear increase of M/L from $M_V^T \simeq -10$ up to -12 , saturating at the level of $\sim 5 - 6$

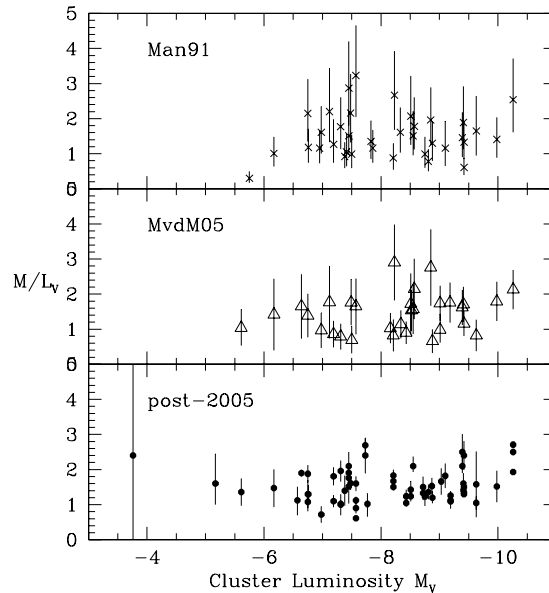


Figure 3. Mass-to-light ratios for Milky Way globular clusters plotted versus GC luminosity, from three different observational eras. Top panel: Mandushev et al. (1991). Middle panel: McLaughlin & van der Marel (2005). Bottom panel: Dynamically based measurements from a variety of individual studies (see text). The low-luminosity clusters NGC 6535 and Pal 13 do not appear on the plot; see Table 1.

appropriate for UCDs and dE’s. The ‘baseline’ at $M/L_V = 1.3$ is chosen to match the observed data for Milky Way clusters. At very low luminosity, the mass-to-light ratio should increase again because low-mass and highly dynamically evolved clusters should become relatively more dominated by binary stars and stellar remnants (cf. the datapoint for Palomar 13 as an example). However, clusters at the low-mass end are also relatively few in number, and contribute little mass per cluster to the system in any case, so the particular M/L value adopted for them has negligible effects on the total mass of the system M_{GCS} .

REFERENCES

- Alamo-Martínez, K. A., Blakeslee, J. P., Jee, M. J., Côté, P., Ferrarese, L., González-Lópezlira, R. A., Jordán, A., Meurer, G. R., Peng, E. W., & West, M. J. 2013, *ApJ*, 775, 20
- Angus, G. W. & Diaferio, A. 2009, *MNRAS*, 396, 887
- Baumgardt, H. & Mieske, S. 2008, *MNRAS*, 391, 942
- Beasley, M. A., Romanowsky, A. J., Pota, V., Navarro, I. M., Martínez Delgado, D., Neyer, F., & Deich, A. L. 2016, *ApJ*, 819, L20
- Behroozi, P. S., Conroy, C., & Wechsler, R. H. 2010, *ApJ*, 717, 379
- Behroozi, P. S., Wechsler, R. H., & Conroy, C. 2013, *ApJ*, 770, 57
- Bellazzini, M., Dalessandro, E., Sollima, A., & Ibata, R. 2012, *MNRAS*, 423, 844
- Blakeslee, J. P. 1999, *AJ*, 118, 1506
- Blakeslee, J. P., Tonry, J. L., & Metzger, M. R. 1997, *AJ*, 114, 482
- Bland-Hawthorn, J. & Gerhard, O. 2016, *ARA&A*, 54, 529
- Boschin, W., Girardi, M., Spolaor, M., & Barrena, R. 2006, *A&A*, 449, 461
- Bradford, J. D., Geha, M., Muñoz, R. R., Santana, F. A., Simon, J. D., Côté, P., Stetson, P. B., Kirby, E., & Djorgovski, S. G. 2011, *ApJ*, 743, 167
- Cole, D. R., Dehnen, W., Read, J. I., & Wilkinson, M. I. 2012, *MNRAS*, 426, 601
- Colless, M. & Dunn, A. M. 1996, *ApJ*, 458, 435
- D’Abrusco, R., Cantiello, M., Paolillo, M., Pota, V., Napolitano, N. R., Limatola, L., Spavone, M., Grado, A., Iodice, E., Capaccioli, M., Peletier, R., Longo, G., Hilker, M., Mieske, S., Grebel, E. K., Lisker, T., Wittmann, C., van de Ven, G., Schipani, P., & Fabbiano, G. 2016, *ApJ*, 819, L31
- Diakogiannis, F. I., Lewis, G. F., & Ibata, R. A. 2014, *MNRAS*, 437, 3172
- Dirsch, B., Richtler, T., Geisler, D., Forte, J. C., Bassino, L. P., & Gieren, W. P. 2003, *AJ*, 125, 1908
- Drinkwater, M. J., Gregg, M. D., & Colless, M. 2001, *ApJ*, 548, L139
- Durrell, P. R., Côté, P., Peng, E. W., Blakeslee, J. P., Ferrarese, L., Mihos, J. C., Puzia, T. H., Lançon, A., Liu, C., Zhang, H., Cuillandre, J.-C., McConnachie, A., Jordán, A., Accetta, K., Boissier, S., Boselli, A., Courteau, S., Duc, P.-A., Emsellem, E., Gwyn, S., Mei, S., & Taylor, J. E. 2014, *ApJ*, 794, 103
- Eadie, G. M. & Harris, W. E. 2016, *ApJ*, 829, 108
- Elmegreen, B. G., Malhotra, S., & Rhoads, J. 2012, *ApJ*, 757, 9
- Falco, M., Hansen, S. H., Wojtak, R., Brinckmann, T., Lindholmer, M., & Pandolfi, S. 2014, *MNRAS*, 442, 1887
- Forbes, D. A., Alabi, A., Romanowsky, A. J., Brodie, J. P., Strader, J., Usher, C., & Pota, V. 2016, *MNRAS*, 458, L44
- Gavazzi, R., Adami, C., Durret, F., Cuillandre, J.-C., Ilbert, O., Mazure, A., Pelló, R., & Ulmer, M. P. 2009, *A&A*, 498, L33
- Gebhardt, K. & Beers, T. C. 1991, *ApJ*, 383, 72

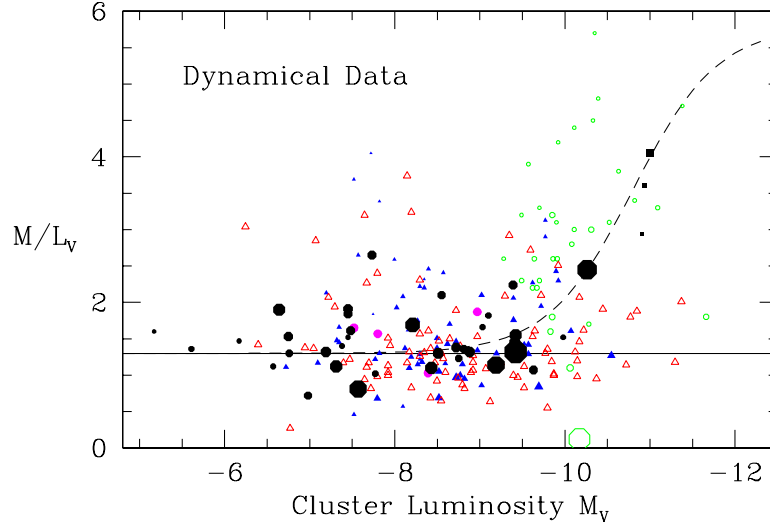


Figure 4. Dynamically measured mass-to-light ratios M/L_V in Solar units, for globular clusters in several galaxies. *Solid dots:* Milky Way; *blue triangles:* M31 GCs with $[Fe/H] < -1.0$; *open green circles:* NGC 5128 GCs; *magenta dots:* M33 GCs; and *solid squares:* M87 GCs and M31-G1. Literature sources are given in the text. Larger symbol sizes correspond to smaller internal measurement uncertainties. The solid line at $M/L_V = 1.3$ is the weighted mean value for the Milky Way GCs excluding NGC 5139 (ω Cen) and NGC 6535, while the dashed line is the interpolation function stated in the text.

Georgiev, I. Y., Puzia, T. H., Goudfrooij, P., & Hilker, M. 2010, MNRAS, 406, 1967
 Griffen, B. F., Drinkwater, M. J., Thomas, P. A., Helly, J. C., & Pimblett, K. A. 2010, MNRAS, 405, 375
 Hasegan, M., Jordán, A., Côté, P., Djorgovski, S. G., McLaughlin, D. E., Blakeslee, J. P., Mei, S., West, M. J., Peng, E. W., Ferrarese, L., Milosavljević, M., Tonry, J. L., & Merritt, D. 2005, ApJ, 627, 203
 Harris, W. E. 1996, AJ, 112, 1487
 —. 2016, AJ, 151, 102
 Harris, W. E., Harris, G. L., & Hudson, M. J. 2015, ApJ, 806, 36
 Harris, W. E., Harris, G. L. H., & Alessi, M. 2013, ApJ, 772, 82
 Harris, W. E., Morningstar, W., Gnedin, O. Y., O’Halloran, H., Blakeslee, J. P., Whitmore, B. C., Côté, P., Geisler, D., Peng, E. W., Bailin, J., Rothberg, B., Cockcroft, R., & Barber DeGraaff, R. 2014, ApJ, 797, 128
 Harris, W. E. & Pudritz, R. E. 1994, ApJ, 429, 177
 Howard, C. S., Pudritz, R. E., & Harris, W. E. 2016, MNRAS, 461, 2953
 Hudson, M. J., Gillis, B. R., Coupon, J., Hildebrandt, H., Erben, T., Heymans, C., Hoekstra, H., Kitching, T. D., Mellier, Y., Miller, L., Van Waerbeke, L., Bonnett, C., Fu, L., Kuijken, K., Rowe, B., Schrabback, T., Semboloni, E., van Uitert, E., & Veldander, M. 2015, MNRAS, 447, 298
 Hudson, M. J., Harris, G. L., & Harris, W. E. 2014, ApJ, 787, L5

Hughes, J. P. 1989, ApJ, 337, 21
 Jauzac, M., Eckert, D., Schwinn, J., Harvey, D., Baugh, C. M., Robertson, A., Bose, S., Massey, R., Owers, M., Ebeling, H., Shan, H. Y., Jullo, E., Kneib, J.-P., Richard, J., Atek, H., Clément, B., Egami, E., Israel, H., Knowles, K., Limousin, M., Natarajan, P., Rexroth, M., Taylor, P., & Tchernin, C. 2016, MNRAS, 463, 3876
 Jordán, A., McLaughlin, D. E., Côté, P., Ferrarese, L., Peng, E. W., Blakeslee, J. P., Mei, S., Villegas, D., Merritt, D., Tonry, J. L., & West, M. J. 2006, ApJ, 651, L25
 Jordán, A., Peng, E. W., Blakeslee, J. P., Côté, P., Eyheramendy, S., & Ferrarese, L. 2015, ApJS, 221, 13
 Kamann, S., Husser, T.-O., Brinchmann, J., Emsellem, E., Weilbacher, P. M., Wisotzki, L., Wendt, M., Krajnović, D., Roth, M. M., Bacon, R., & Dreizler, S. 2016, A&A, 588, A149
 Kamann, S., Wisotzki, L., Roth, M. M., Gerßen, J., Husser, T.-O., Sandin, C., & Weilbacher, P. 2014, A&A, 566, A58
 Katz, H. & Ricotti, M. 2014, MNRAS, 444, 2377
 Kimmig, B., Seth, A., Ivans, I. I., Strader, J., Caldwell, N., Anderton, T., & Gregersen, D. 2015, AJ, 149, 53
 Koda, J., Yagi, M., Yamanoi, H., & Komiyama, Y. 2015, ApJ, 807, L2
 Kravtsov, A. V. & Gnedin, O. Y. 2005, ApJ, 623, 650
 Kruijssen, J. M. D. 2008, A&A, 486, L21
 —. 2015, MNRAS, 454, 1658

- Kruijssen, J. M. D. & Mieske, S. 2009, *A&A*, 500, 785
- Kubo, J. M., Stebbins, A., Annis, J., Dell'Antonio, I. P., Lin, H., Khiabani, H., & Frieman, J. A. 2007, *ApJ*, 671, 1466
- Küpper, A. H. W., Balbinot, E., Bonaca, A., Johnston, K. V., Hogg, D. W., Kroupa, P., & Santiago, B. X. 2015, *ApJ*, 803, 80
- Larsen, S. S., Brodie, J. P., Sarajedini, A., & Huchra, J. P. 2002, *AJ*, 124, 2615
- Leauthaud, A., Tinker, J., Bundy, K., Behroozi, P. S., Massey, R., Rhodes, J., George, M. R., Kneib, J.-P., Benson, A., Wechsler, R. H., Busha, M. T., Capak, P., Cortés, M., Ilbert, O., Koekemoer, A. M., Le Fèvre, O., Lilly, S., McCracken, H. J., Salvato, M., Schrabback, T., Scoville, N., Smith, T., & Taylor, J. E. 2012, *ApJ*, 744, 159
- Lee, M. G. & Jang, I. S. 2016, *ArXiv e-prints*
- Li, H. & Gnedin, O. Y. 2014, *ApJ*, 796, 10
- Li, H., Gnedin, O. Y., Gnedin, N. Y., Meng, X., Semenov, V. A., & Kravtsov, A. V. 2016, *ArXiv e-prints*
- Licquia, T. C., Newman, J. A., & Brinchmann, J. 2015, *ApJ*, 809, 96
- Lokas, E. L. & Mamon, G. A. 2003, *MNRAS*, 343, 401
- Lützgendorf, N., Kissler-Patig, M., Gebhardt, K., Baumgardt, H., Noyola, E., Jalali, B., de Zeeuw, P. T., & Neumayer, N. 2012, *A&A*, 542, A129
- Lützgendorf, N., Kissler-Patig, M., Noyola, E., Jalali, B., de Zeeuw, P. T., Gebhardt, K., & Baumgardt, H. 2011, *A&A*, 533, A36
- Mackey, A. D. & Gilmore, G. F. 2003, *MNRAS*, 340, 175
- Mandushev, G., Staneva, A., & Spasova, N. 1991, *A&A*, 252, 94
- Marín-Franch, A. & Aparicio, A. 2002, *ApJ*, 568, 174
- Martinez, G. D. 2015, *MNRAS*, 451, 2524
- Martini, P. & Ho, L. C. 2004, *ApJ*, 610, 233
- McLaughlin, D. E. 1999a, *ApJ*, 512, L9
- . 1999b, *AJ*, 117, 2398
- McLaughlin, D. E. & van der Marel, R. P. 2005, *ApJS*, 161, 304
- Meylan, G., Sarajedini, A., Jablonka, P., Djorgovski, S. G., Bridges, T., & Rich, R. M. 2001, *AJ*, 122, 830
- Mieske, S., Hilker, M., Jordán, A., Infante, L., Kissler-Patig, M., Rejkuba, M., Richtler, T., Côté, P., Baumgardt, H., West, M. J., Ferrarese, L., & Peng, E. W. 2008, *A&A*, 487, 921
- Mihos, J. C., Durrell, P. R., Ferrarese, L., Feldmeier, J. J., Côté, P., Peng, E. W., Harding, P., Liu, C., Gwyn, S., & Cuillandre, J.-C. 2015, *ApJ*, 809, L21
- Montes, M. & Trujillo, I. 2014, *ApJ*, 794, 137
- Moore, B., Diemand, J., Madau, P., Zemp, M., & Stadel, J. 2006, *MNRAS*, 368, 563
- Moster, B. P., Naab, T., & White, S. D. M. 2013, *MNRAS*, 428, 3121
- Muñoz, R. P., Eigenthaler, P., Puzia, T. H., Taylor, M. A., Ordenes-Briceno, Y., Alamo-Martínez, K., Ribbeck, K. X., Ángel, S., Capaccioli, M., Côté, P., Ferrarese, L., Galaz, G., Hempel, M., Hilker, M., Jordán, A., Lançon, A., Mieske, S., Paolillo, M., Richtler, T., Sánchez-Janssen, R., & Zhang, H. 2015, *ApJ*, 813, L15
- Nasonova, O. G., de Freitas Pacheco, J. A., & Karachentsev, I. D. 2011, *A&A*, 532, A104
- Okabe, N., Futamase, T., Kajisawa, M., & Kuroshima, R. 2014, *ApJ*, 784, 90
- Oldham, L. J. & Auger, M. W. 2016, *MNRAS*, 457, 421
- Owers, M. S., Randall, S. W., Nulsen, P. E. J., Couch, W. J., David, L. P., & Kempner, J. C. 2011, *ApJ*, 728, 27
- Paolillo, M., Fabbiano, G., Peres, G., & Kim, D.-W. 2002, *ApJ*, 565, 883
- Peñarrubia, J., McConnachie, A. W., & Navarro, J. F. 2008, *ApJ*, 672, 904
- Peng, E. W., Ferguson, H. C., Goudfrooij, P., Hammer, D., Lucey, J. R., Marzke, R. O., Puzia, T. H., Carter, D., Balcells, M., Bridges, T., Chiboucas, K., del Burgo, C., Graham, A. W., Guzmán, R., Hudson, M. J., Matković, A., Merritt, D., Miller, B. W., Mouhcine, M., Phillipps, S., Sharples, R., Smith, R. J., Tully, B., & Verdoes Kleijn, G. 2011, *ApJ*, 730, 23
- Peng, E. W. & Lim, S. 2016, *ApJ*, 822, L31
- Purcell, C. W., Bullock, J. S., & Zentner, A. R. 2007, *ApJ*, 666, 20
- Rejkuba, M. 2012, *Ap&SS*, 341, 195
- Rejkuba, M., Dubath, P., Minniti, D., & Meylan, G. 2007, *A&A*, 469, 147
- Rines, K., Geller, M. J., Kurtz, M. J., & Diaferio, A. 2003, *AJ*, 126, 2152
- Schombert, J. & Smith, A. K. 2012, *PASA*, 29, 174
- Schuberth, Y., Richtler, T., Hilker, M., Dirsch, B., Bassino, L. P., Romanowsky, A. J., & Infante, L. 2010, *A&A*, 513, A52
- Scott, N., Graham, A. W., & Schombert, J. 2013, *ApJ*, 768, 76
- Shanahan, R. L. & Gieles, M. 2015, *MNRAS*, 448, L94
- Sollima, A., Bellazzini, M., & Lee, J.-W. 2012, *ApJ*, 755, 156
- Spitler, L. R. & Forbes, D. A. 2009, *MNRAS*, 392, L1
- Strader, J., Caldwell, N., & Seth, A. C. 2011, *AJ*, 142, 8
- Strigari, L. E., Bullock, J. S., Kaplinghat, M., Kravtsov, A. V., Gnedin, O. Y., Abazajian, K., & Klypin, A. A. 2006, *ApJ*, 652, 306
- Taylor, M. A., Puzia, T. H., Harris, G. L., Harris, W. E., Kissler-Patig, M., & Hilker, M. 2010, *ApJ*, 712, 1191
- Tonini, C. 2013, *ApJ*, 762, 39
- Umetsu, K., Sereno, M., Medezinski, E., Nonino, M., Mroczkowski, T., Diego, J. M., Ettori, S., Okabe, N., Broadhurst, T., & Lemze, D. 2015, *ApJ*, 806, 207
- van de Ven, G., van den Bosch, R. C. E., Verolme, E. K., & de Zeeuw, P. T. 2006, *A&A*, 445, 513
- van den Bosch, R., de Zeeuw, P. T., Gebhardt, K., Noyola, E., & van de Ven, G. 2006, *ApJ*, 641, 852
- van Dokkum, P., Abraham, R., Brodie, J., Conroy, C., Danieli, S., Merritt, A., Mowla, L., Romanowsky, A., & Zhang, J. 2016, *ApJ*, 828, L6
- van Dokkum, P. G., Abraham, R., Merritt, A., Zhang, J., Geha, M., & Conroy, C. 2015, *ApJ*, 798, L45
- Villegas, D., Jordán, A., Peng, E. W., Blakeslee, J. P., Côté, P., Ferrarese, L., Kissler-Patig, M., Mei, S., Infante, L., Tonry, J. L., & West, M. J. 2010, *ApJ*, 717, 603
- Wang, W., Han, J., Cooper, A. P., Cole, S., Frenk, C., & Lowing, B. 2015, *MNRAS*, 453, 377
- Watkins, L. L., van de Ven, G., den Brok, M., & van den Bosch, R. C. E. 2013, *MNRAS*, 436, 2598
- Zaritsky, D., Colucci, J. E., Pesse, P. M., Bernstein, R. A., & Chandar, R. 2014, *ApJ*, 796, 71
- Zocchi, A., Bertin, G., & Varri, A. L. 2012, *A&A*, 539, A65
- Zonoozi, A. H., Haghi, H., & Kroupa, P. 2016, *ApJ*, 826, 89